Journal Name

ARTICLE

Published in: NewJ. Chem., 2017, 41, 10101

DOI: 10.1039/x0xx00000x

www.rsc.org/

Double decker luminescent Ytterbium and Erbium SMMs with symmetric and asymmetric Schiff base ligands

Samira Gholizadeh Dogaheh,[b] Hamid Khanmohammadi,[b] E. Carolina Sañudo[a,c,*]

Multifunctional molecules, that respond both to magnetic fields and light are object of study due to possible applications in fields as diverse as imaging or information processing and storage. In this paper we report visible and NIR emitting single-molecule magnets (SMMs) of Yb(III) and Er(III) with symmetric (SYML) and asymmetric (AZOL) Schiff base ligands. The complexes prepared SYML-Ln2, AZOL-Ln3 (Ln = Er, Yb) are SMMs, with the exception of AZOL-Yb3, with a relaxation behavior dominated by quantum tunneling of the magnetization. The multi-level double-decker structure of the complexes is ideal for surface deposition in carbon-based materials.

Introduction

Molecular magnetism has been growing exponentially since the 1990's. The discovery of single molecule magnets (SMMs) by Christou, Gatteschi and Sessoli[1] among others was a key milestone in the development of molecular magnetism as we know it today. SMMs are molecules that can retain the magnetization upon removal of an applied field: this property makes them ideal candidates for technological applications in information storage or the new proposals of molecular spintronic devices.[2–8] Additionally, the discovery of SMMs was key in the realization of quantum properties in bulk materials: with SMMs quantum effects like quantum tunneling of the magnetization (QTM) could be studied and thus, new applications like the use of SMMs and other molecular nanomagnets (MNMs) in quantum computing were proposed.[3–5,9] Classical SMMs are high nuclearity transition metal complexes. The limits in effective working temperatures were clear: hysteresis of the magnetization was only observed at very low temperatures, usually below 4 K or even below the limit of most commercial Helium cryostats of 2 K. In order to overcome these difficulties 3d-4f complexes[10] and lanthanide complexes[11] were proposed to improve the previously observed SMM properties. The main assumption was that the spin-orbit coupling of lanthanide ions could help in improving the anisotropy of the resulting complexes. A breakthrough was the report of the first Single Ion Magnets (SIMs) by Ishikawa.[12] These complexes were Tb and Dy double decker complexes of the well-known phthalocyanine ligand. After this publication, many others came reporting even higher temperatures for the peaks in the out-of-phase ac magnetic susceptibility and record energy barriers.[13,14] However large the energy barrier it is still unusual to observe hysteresis of the magnetization above 4 K due to relaxation enhancement by QTM.[15] Low operational temperatures are not the only challenges that using SMMs for applications entail. It is understood that researchers must finds ways to switch on/off a desired property (magnetic interaction, QTM, spin crossover, etc...) in order to use molecular systems in devices. Additionally, one must be able to address these molecules while on a surface or integrated in a device.[16–19] These are not easy challenges and many research efforts are now thrown at tackling these problems. In this context, there is a great interest in preparing multifunctional compounds that combine magnetic and optical properties with the ultimate goal of having synergy between them or ideally, the possibility of controlling QTM and magnetic properties with light. In the last year, two publications have called attention to this topic.[20] Roubeau and co-workers report the photo switch of SMM properties on a spin crossover complex[21] while Gao, Wang and co-workers reported the thermostability and photoluminescence of Dy(III) single-molecule magnets under a magnetic field.[22] THe R groups of the iminie ligand, naphtol and a diphenyl-azo derivative were chosen for the stability they provide to the Schiff base ligand and the photoluminescent properties they add to the complex. The diphenyl-azo moiety is extremely well studied and ubiquitous in industry. Azo-dyes have many practical applications. In the last few years, azobenzenes have been studied for potential applications in areas of nonlinear optics, optical storage media, chemosensors, liquid crystals, photochemical molecular switches or molecular shuttles.[23]
In this paper we explore the lanthanide chemistry of an azo-substituted Schiff-base ligand and its symmetric analogue.

Results and discussion

Scheme 1 shows a representation of SYML and AZOL. The synthesis of Schiff base ligands can be easily achieved by condensation of an aldehyde and an amine. For the synthesis of the symmetric Schiff base ligand SYML the condensation reaction of a diamine *o*-phenylendiamine with two equivalents of 2-hydroxy-1-naphthaldehyde was performed in ethanol under reflux. SYML was obtained in good yield and was used without further purification. In order to obtain asymmetric Schiff base ligands the reaction conditions must be carefully controlled. The two-step condensation reaction of *o*-phenylendiamine with two different aldehydes was achieved by controlling the water content of the solvent in a two-step condensation reaction. In this case, ethanol was distilled over molecular sieves and Mg shavings. After the first condensation reaction with 2-hydroxy-1-naphthaldehyde the crystals of the mono-Schiff base ligand were separated by filtration and used in the second condensation. For the asymmetric ligand AZOL the second condensation was performed with and azo-substituted aromatic aldehyde. AZOL was obtained following this two-step procedure in good yield and purity.

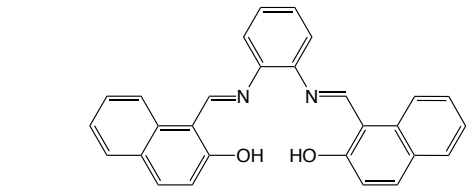

SYML

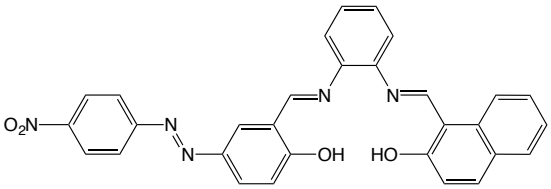

trans-AZOL

Scheme 1. The SYML and AZOL ligands.

The reactions of AZOL and SYML with the lanthanide ions were performed in acetonitrile and using triethylamine to deprotonate the two OH groups of the ligand. In all cases, when AZOL was used a precipitate was obtained and it was not possible to recrystallize it or to obtain crystals directly from the reaction. This fact precluded the structural characterization of the product by single-crystal X-ray diffraction. The cis-trans isomerism of the azo group can easily happen with UV-visible light in solution and it prevents the crystallization of the coordination complex. Mass spectroscopy analysis of the precipitates obtained from the reaction of AZOL with $Ln(NO_3)_3$ (Ln = Er, Yb) in MeCN showed peaks corresponding to the species $[Ln_3(AZOL)_4]^+$ and $[Ln_3(AZOL)_4(H_2O)_2(NO_3)+H^+]^+$ for Ln = Er, Yb, and other fragmentation peaks such as $[Ln_2(AZOL)_3 + H]^+$. The lower M/z peaks were due to fragmentation of the molecular ion. In order to further support this conclusion, reactions were prepared with stoichiometry 3:2 AZOL:Ln and 4:3 AZOL:Ln. Maldi-MS analyses of reaction mixture aliquots of each of the trials showed M/z for the 4:3 AZOL:Ln species and its fragmentation products in all cases, so AZOL-Ln3 is the preferred product of the reaction between AZOL and Ln(III) salts. Elemental analyses of the precipitates, as well as the TGA, IR and SQUID magnetic susceptibility data (*vide infra*) of the complexes AZOL-Ln3 (Ln = Er, Yb) confirmed that there is an extra lanthanide ion, in the form of $Ln(NO_3)_3$. The complete formula for AZOL-Ln is then $[Ln_3(AZOL)_4(H_2O)_2(NO_3)(Ln(NO_3)_3]$ and the proposed structure is that shown in Scheme 2 as an schematic representation. TGA (see Supplementary Information Figure S09) up to 500ºC shows the loss of non-coordinated solvent and coordinated nitrates. This type of structure has been previously observed with similar Schiff base ligand complexes of the lanthanides by Li and co-workers where they report complexes of general formula $[Ln_2(L)_3(solvent)_nLn(NO_3)_3]$ for Yb, Ho, Dy and Tb. [24–27] The $Ln(NO_3)_3$ fragment easily dissociates under MALDI conditions for AZOL-Er3 and AZOL-Yb3.

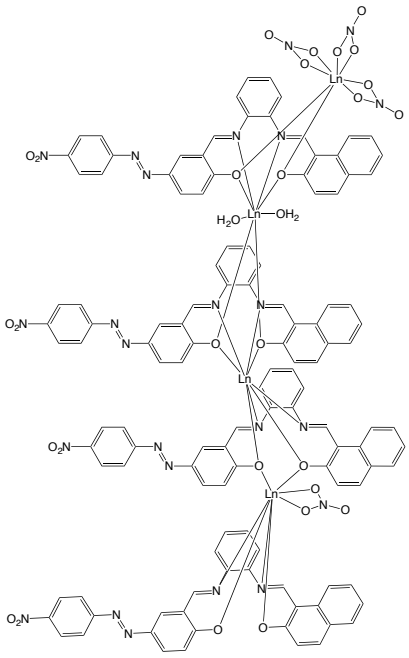

Scheme 2. A proposed structure for AZOL-Ln3 complexes.

The impossibility of obtaining single-crystals of AZOL-Ln3 was one of the reasons to prepare the symmetric version of the ligand, SYML, which should a priori react in a similar way with the lanthanide ions and produce complexes that could be easily crystallized. In fact, an aliquot of the acetonitrile reaction mixture with stoichiometry 1SYML:1Ln was studied by MALDI-TOF mass spectrometry and peaks corresponding to the species $[Ln(SYML)_2+2H]^+$, $[Ln_2(SYML)_3 +H]^+$ and $[Ln_3(SYML)_4]^+$ were found in the spectra for Ln = Yb, Er (see Supplementary Information for the MALDI-TOF spectra for the SYML-Er reaction system). This indicated either a SYML:Ln product with ratio 3:2 and its fragmentation products or the co-existence in the reaction mixture of several species with different SYML:Ln ratio. If the latter were true, in principle the

different species could be isolated in crystalline form by controlling the crystallization conditions. When the MeCN reaction mixture prepared in the stoichiometric ratio for $[Ln_2(SYML)_3(H_2O)]$ is left undisturbed to slowly evaporate orange crystals of the neutral species $[Ln_2(SYML)_3(H_2O)]$ (Ln = Er and Yb) were obtained after a few days. Different cations and anions were added to MeCN reaction mixtures with stoichiometry 2SYML:1Ln and 4SYML:3Ln in order to isolate the other two species. It was not possible to isolate the mononuclear species. We succeeded in obtaining yellow crystals of $(NH_3py)[Ln_3(SYML)_4(NO_3)_2]$ (SYML-Ln3, Ln = Er, and Yb) using 2-aminopyridine in the crystallization. The yields were always very poor, below 5% and the crystals had to be hand-picked from a mixture of orange crystals of SYML-Yb2 or SYML-Er2 and the new yellow complex SYML-Ln3 (Ln = Er, Yb). This fact has precluded the study of the properties of the SYML-Ln3 products. Without the addition of 2-aminopyrdine only orange crystals of the most insoluble of the products, the neutral SYML-Ln2, were obtained. MALDI-TOF MS analysis of the orange crystals showed the expected peak for $[Ln_2(SYML)_3+H]^+$ (see Supplementary Material).

Description of crystal structures

Table 1. Crystallographic and data collection parameters for SYML-Er2, SYML-Yb2, SYML-Er3 and SYML-Yb3 complexes.

	SYML-Er2	SYML-Yb2	SYML-Er3	SYML-Yb3
T/K	100(2)	100(2)	100(2)	100(2)
Crystal system	Triclinic	Triclinic	Monoclinic	Monoclinic
Colour	Orange	Orange	Yellow	Yellow
Space group	Pī	Pī	*P* 21/n	*P* 21/c
a/Å	10.5031(8)	10.4575(4)	13.5774(17)	13.6388(8)
b/Å	18.0711(13)	18.0686(6)	25.425(3)	25.3478(13)
c/Å	18.3906(13)	18.4181(6)	30.838(4)	31.3489(16)
α/°	66.800(3)	66.67(2)	90	90
β/°	73.533(4)	73.605(2)	102.553(8)	101.535(3)
γ/°	85.947(4)	85.41(2)	90	90
V/Å^3	3073.4(4)	3063.17(19)	10391(2)	10618.8(10)
Z	2	2	4	4
Radiation	MoKα	MoKα	MoKα	MoKα
Gof on F^2	1.039	0.953	1.081	1.021
Final R [I>=2σ (I)]	R_1 = 0.0329, wR_2 = 0.0769	R_1 = 0.0451, wR_2 = 0.0867	R_1 = 0.074, wR_2 = 0.1723	R_1 = 0.0614, wR_2 = 0.1673

Single crystals of SYML-Er2 and SYML-Yb2 suitable for X-ray diffraction analysis were obtained by slow evaporation of CH_3CN. Crystallographic data and data collection details for Er^{3+} and Yb^{3+} complexes are presented in Table 1. SYML-Er2 and SYML-Yb2 crystallize in the triclinic space group *P*ī. The two complexes are isostructural and only SYML-Er2 is shown here. Figures for packing of SYML-Er2 and SYML-Yb2 can be found in the Supplementary Material. The asymmetric unit consists of one full complex and a molecule of solvation water. The complex can be described as a double-double decker complex or double sandwich. The Schiff base ligands actively use the two oxygen donors to bridge two lanthanides. The coordination spheres of the two lanthanides in the complex are not equal. As shown in Figure 1, one lanthanide ion, Er1 ion in SYML-Er2 and Yb1 in SYML-Yb2, is located in a O_4N_4 coordination pocket of two completely deprotonated SYML ligands. The other lanthanide ion, Yb2 and Er2, is in a O_5N_2 coordination pocket with two nitrogen and four oxygen atoms of SYML ligands and one coordinated water molecule. The Er1 and Yb1 atoms are octacoordinated with a distorted square antiprism (SAP) coordination polyhedron whereas Er2 and Yb2 are heptacoordinated with a distorted capped trigonal prism coordination polyhedron. The Ln-O and Ln-N bond lengths have normal values for Ln(III) complexes of Er and Yb. There is a water of crystallization, this water is hydrogen bonding the coordinated water molecule, with O-H··O distance of 2.723 Å.

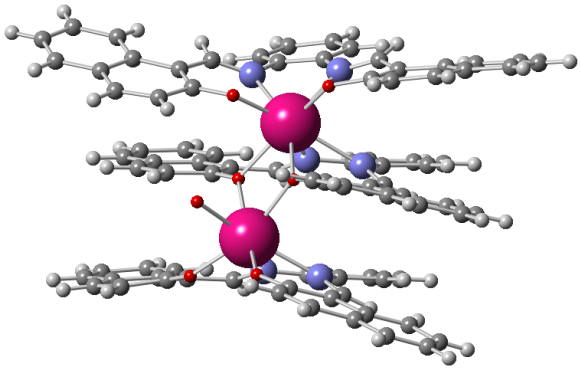

Figure 1. Crystal structure of the SYML-Er2 anion. Carbon: grey, Hydrogen: light grey, Oxygen: red, Nitrogen: blue, Erbium: pink.

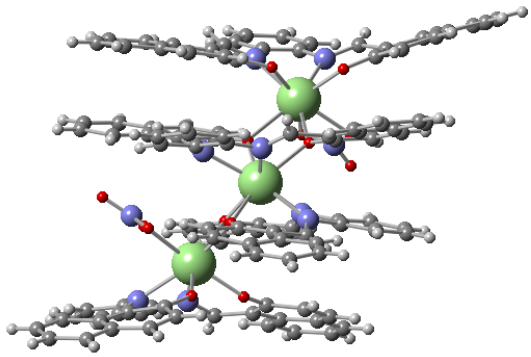

Figure 2. Crystal structure of the SYML-Yb3 anion. Carbon: grey, Hydrogen: light grey, Oxygen: red, Nitrogen: blue, Ytterbium: green.

Crystallographic data and data collection details for SYML-Ln3 (Ln = Er^{3+} and Yb^{3+}) are presented in Table 1. Figure 2 shows the crystal structure of SYML-Yb3. SYML-Yb3 and SYML-Er3 are isostructural and only SYML-Yb3 is shown here. Similar figures for SYML-Er3 can be found in the Supplementary Material. In the presence of 2-aminopyridine the reaction mixtures of SYML and the lanthanide nitrate of Er and Yb lead to the formation of the SYML-Er3 and SYML-Yb3 metal complexes. These crystals are yellow plates, and they appeared as a minor product, while orange blocks of SYML-Ln2 also formed. SYML-Yb3 crystallizes in the monoclinic *P*21/c space group. The asymmetric unit consists of one full complex, protonated 2-aminopyridine as counter ion and solvent molecules. The central lanthanide ion coordination sphere is unique, Yb1 or Er1 respectively in SYML-Yb3 and SYML-Er3, while the other

two lanthanides have the same coordination sphere. As shown in Figure 2, the Yb2 and Yb3 or Er2 and Er3 ions in the complex are located in the O_6N_2 coordination pockets with two nitrogen and four oxygen atoms of the SYML ligand and one coordinated nitrate. Yb1 (and Er1) is located in a N_4O_4 coordination sphere of two completely deprotonated SYML ligands with a distorted square antiprism coordination polyhedron. The Yb2 and Yb3 atoms (or Er2 and Er3 in SYML-Er3) are octacoordinated with a distorted bi-capped trigonal prism coordination polyhedron.

The single crystal characterization of the orange species SYML-Yb2 and SYML-Er2 showed that these are sandwich triple decker type complexes, similar to those prepared with the phthalocyanine ligands and the lanthanide ions[28] and to reported complexes with other Schiff base ligands. Homoleptic phthalocycanine complexes and heteroleptic complexes with Schiff base ligands in combination with phthalocyanines have similar triple decker structures. [29–32] Homoleptic, heteroleptic and polymeric complexes with Schiff base and other ligands such as acetate that display the basic double-decker unit seen in SYML-Ln2 (Ln = Er, Yb) were reported by Li and coworkers.[24–27,33] Some of the complexes reported by Li also have a capping $Ln(NO_3)_3$ metalloligand, something we have not observed for the SYML complexes of the lanthanide ions. Furthermore, we have isolated the new species SYML-Yb3 and SYML-Er3, in which a new SYML-Ln layer is added to obtain a quadruple decker complex with three metals and four SYML ligands. The double decker type of structures, with two nearly planar ligands above and below a Er(III) or Yb(III) ion, should display a relatively well isolated M_J ground state[34] based on the angular dependence of the M_J substates. This is particularly important for Yb(III) and it should affect the photophysical and magnetic properties of the complexes, as we show in the following sections.

Electronic spectra and emission properties

UV–Vis absorption spectra and luminescent properties of the free ligands AZOL and SYML, as well of their lanthanide complexes, were studied in solution. The electronic spectra are shown in Figures 3 and 4. Emission properties in the near IR of the AZOL-Ln3 and SYML-Ln2 complexes were also studied in the solid state. The AZOL absorption spectrum of AZOL-Ln3 complexes and AZOL have strong absorption bands between 220 and 300 nm with a sharp maximum at 238 nm related to the aromatic groups and π - π* transition of the nitro substituent. For the AZOL there is a broad absorption band in the UV-Visible region, with maxima at 320 nm and 381 nm (λ_{max}: 320 nm, ε: 2365 L $mol^{-1}cm^{-1}$, λ_{max}: 381 nm, ε: 31725 L $mol^{-1}cm^{-1}$), related to the symmetry allowed π - π* transition of the aromatic systems that overlaps with the band from the N=N chromophore.[35,36] A much weaker band in the visible region (λ_{max}: 480 nm, ε: 8500 L $mol^{-1}cm^{-1}$) is related to the phenol and imine group, and the diphenylazo moiety of the ligand. Lanthanide coordination to the AZOL ligand causes a deprotonation of the phenol group of AZOL. The formation of the AZOL-Er3 and AZOL-Yb3 complexes results in a red-shift of this absorption band and an increase of the absorption coefficient. The absorption bands appear at 430 nm (ε: 34750 L mol^{-1} cm^{-1}) and 420 nm (ε: 35025 L mol^{-1} cm^{-1}) respectively for AZOL-Er3 and AZOL-Yb3.

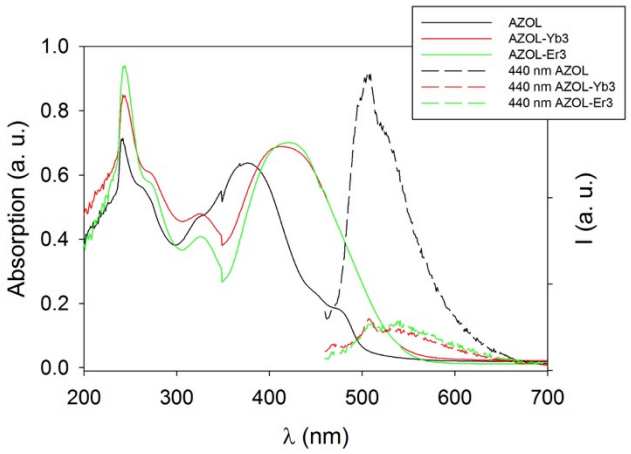

Figure 3. Electronic and emission spectra of CH_3CN solutions at room temperature of AZOL and AZOL-Ln3 complexes (Ln = Er, Yb) (excitation wavelength 440 nm).

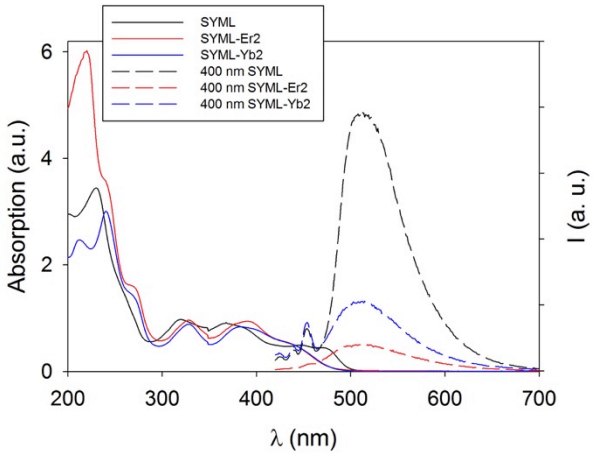

Figure 4. Electronic and emission spectra of CH_3CN solutions at room temperature of SYML and SYML-Ln2 complexes (Ln = Er, Yb). Excitation wavelength 400 nm.

The absorption changes of the azo-containing species AZOL, AZOL-Er3 and AZOL-Yb3 upon photo-irradiation were examined in order to observe the *cis*↔*trans* interconversion of the azo group. In principle, this process can be controlled by irradiating at the necessary wavelength with an intense monochromatic source.[23,37] In the complexes and ligand reported here, AZOL and AZOL-Ln3, *cis*↔*trans* isomerization could not be clearly established from the electronic spectra or observed with the naked eye. The spectra after irradiation are shown in the supplementary information Figure S05 as dashed lines, the changes observed were subtle: a decrease of intensity of the visible absorption band and an increase in the intensity of the UV absorption band plus a small blue-shift.

UV–Vis spectra for SYML, SYML-Yb2 and SYML-Er2 complexes in CH_3CN solution at room temperature are shown in Figure 4. The SYML absorption spectrum consists of four bands. The

strong bands (λ_{max}: 319 nm, ε: 22750 L $mol^{-1}cm^{-1}$ and λ_{max}: 370 nm, ε: 21345 L $mol^{-1}cm^{-1}$) arise from the symmetry allowed π - π* transitions. The much weaker bands in the visible region (λ_{max}: 454 nm, ε: 12000 L mol^{-1} cm^{-1} and λ_{max}: 476 nm, ε: 10300 L mol^{-1} cm^{-1}) are related to the chromophores that coordinate to the metal, phenol and imine. The deprotonation of the OH groups and the coordination of the lanthanide ion to the imine and phenoxide groups is clearly seen in the UV-Vis spectra. The electronic spectra SYML-Er2 and SYML-Yb2 shows the coalescence of the visible bands, which are blue-shifted with respect to the free SYML spectrum and the red-shift of the 370 nm absorption of free SYML. The bands observed are λ_{max}: 331 nm, ε: 30050 L mol^{-1} cm^{-1} and λ_{max}: 395nm, ε: 29450 L mol^{-1} cm^{-1} for SYML-Er2 and λ_{max}: 331 nm, ε: 23900 L mol^{-1} cm^{-1} and λ_{max}: 388nm, ε: 24900 L mol^{-1} cm^{-1} for SYML-Yb2.

All emission spectra were collected at room temperature in acetonitrile solutions of the ligand or complexes and are shown in Figure 3. Emission spectra for AZOL were collected on a 2×10^{-5} M solution in CH_3CN. Upon irradiation at 440 nm a strong emission band at 520 nm was observed. Upon coordination to Yb and Er, the emission spectra broadened and lost definition and intensity. As shown in Figure 3 the emission band practically disappeared: when the AZOL ligand is coordinated to Er(III) and Yb(III) the fluorescence is heavily quenched. This has been reported earlier for complexes of paramagnetic metals and fluorescent ligands and is referred to as chelation enhancement of quenching of emission (CHEQ) effect.[20,38] The quantum yield of emission for AZOL-Ln3 was below 0.1%. A fluorescent emission band from the SYML at 510 nm was observed upon irradiation at 440 nm of 2×10^{-7} M solutions of SYML in CH_3CN (supplementary Information Figure S06). Figure 4 shows emission spectra in solution for SYML and SYML-Ln2 upon irradiation at 400 nm. In the emission spectra of the Er^{3+} and Yb^{3+} complexes of SYML, SYML-Er2 and SYML-Yb2 the quenching of the fluorescence is clear, as was observed for the emission spectra of AZOL-Ln3 complexes. Upon excitation at 400 nm, the quantum yield for the emission band was 0.8 % for the free ligand SYML and 0.3 % and 0.3 % for SYML-Er2 and SYML-Yb2 respectively.

The combination of lanthanide ions with fluorescent ligands results in materials that will absorb light in the UV-Vis region of the spectrum and will emit both in the UV-Vis due to the ligand and the visible and/or near IR due to the lanthanide ion. The organic ligand is said to act as an antenna, harvesting the light and transferring it to the lanthanide ion.[39,40] In this way the low molar absorptivity of the lanthanide 4f levels can be overcome.[41] The complexes SYML-Ln2 (Ln = Er, Yb) reported here have two lanthanide ions that have different coordination spheres. One is coordinated by two ligands while the other is also coordinated to a molecule of water. It is known that coordinated water is particularly efficient quenching the emission of the lanthanide.[40] The situation of AZOL-Ln3 (Ln = Er, Yb) is similar: there are two distinct environments, the central lanthanide is coordinated to two ligands while the other three lanthanide ions are bound to terminal ligands that can be easily exchanged in solution. NIR photoluminescence experiments on SYML-Ln2 and AZOL-Ln3 were performed at room temperature in the solid state and in CH_3CN solution. The free ligands AZOL and SYML did not display NIR luminescence under similar conditions. Upon excitation in the ligand-centered transitions, from 300 to 500 nm, characteristic emission bands of Yb(III) were observed in the NIR emission spectra of SYML-Yb2 and AZOL-Yb3, in addition to the weak emission from the ligand. When excited at 420 nm, a narrow signal at 976 nm that corresponds to the $^2F_{5/2}\rightarrow{}^2F_{7/2}$ electronic transition was revealed for both complexes AZOL-Yb3 and SYML-Yb2 in solid state, as shown in Figure 5. Several broad bands spanned approximately 700 cm^{-1} in the energy spectrum accompanied this band. A similar splitting has already observed in Yb(III) chelate compounds.[50–52] The lower energy bands are consequence of the M_J splitting of the excited and fundamental Yb(III) states due to the low symmetry crystal field.[43] Pope, Colacio and co-workers report the NIR emission of a dinuclear Yb(III) complex and they assign the band at the lower energy (circa. 1050 nm) to either vibronic coupling or to the Yb(III)-Yb(III) coupling effect on the M_J level splitting of the $^2F_{7/2}$ multiplet.[53] The energy span of the NIR bands, that is directly related to the crystal field splitting of the $^2F_{7/2}$ multiplet observed for our compounds is similar to that observed for other mononuclear[54] and dinuclear complexes with similar O-N donor ligands.[53] NIR luminescence was also observed for AZOL-Yb3 and SYML-Yb2 in $2x10^{-5}$ M CH_3CN solution at room temperature. For SYML-Er2 and AZOL-Er3 excitation in the ligand centered region 300-500 nm did not lead to the expected NIR-emission attributed to the $^4I_{13/2}\rightarrow{}^4I_{15/2}$ transition of the Er^{3+} ion.[55] Irradiation at 590 nm did result in a very broad NIR emission peak centered at 1475 nm for AZOL-Er3 and 1490 nm for SYML-Er2 that is characteristic of Er(III) (see Supplementary Information Figure S07). Similar NIR emission spectra were observed for $2x10^{-5}$ M solutions in MeCN. In all cases, NIR emission was weak. Thus in the complexes reported here the sensitization process via the electronic structure of the ligands was not very efficient.

The crystal field splitting of the M_J sublevels observed for SYML-Yb2 and AZOL-Yb3 is similar to that calculated by Ishikawa[42] and Bünzli[43] for Yb(III) complexes with phthalocyanine and other N-donor ligands, and by Pointillart and co-workers for a redox active Yb(III) SMM.[44] For mononuclear Yb(III) complexes it is possible to extract crystal field parameters from the NIR spectra, in particular if NIR is measured at low temperature and to use these parameters to model the observed magnetic data. The NIR emission of Yb(III) gives access to direct information on splitting of the $^2F_{7/2}$ multiplet by the ligand field. Pointillart and coworkers, among others, do so for several mononuclear luminescent SMMs.[45,44,46–48] Tong *et al* report a half-sandwich distorted Yb(III) mononuclear SMM and they extract crystal field splitting data from the NIR emission.[49] A detailed analysis as that performed on mononuclear species by Pointillart *et al* cannot be done in polynuclear species with inequivalent Yb(III) sites as SYML-Yb2, however the energy span of the peaks observed in NIR can be compared to the splitting obtained from analyzing magnetic data.

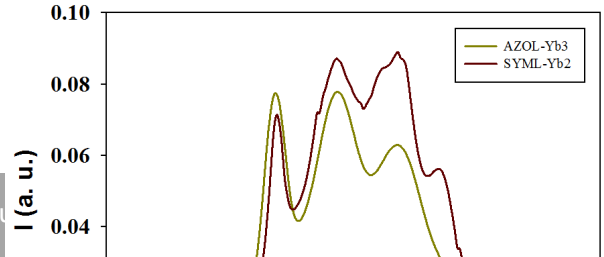

Figure 5. Solid state NIR emission of AZOL-Yb3 and SYML-Yb2 upon excitation by 480 nm light at room temperature.

Magnetic properties

Magnetic susceptibility data were collected for SYM-Er2, SYM-Yb2, AZOL-Er3 and AZOL-Yb3 complexes at two different applied dc fields in the 2-300 K temperature range. It is worth to remind the reader that for the AZOL-Ln3 complexes there are actually four lanthanide ions per complex, one of them as a $Ln(NO_3)_3$ metalloligand. Data are shown as χT vs. T plots in Figures 6 and 7. The χT product at 300 K for all samples is in good agreement with the expected values for the proposed complex formulae (Er(III): $4f^{11}$, $^4I_{15/2}$, S = 3/2, gJ = 6/5; Yb(III) $4f^{13}$, $^2F_{7/2}$, S = ½, gJ = 8/7). For all the examined complexes, the χT product is non-field dependent. As temperature goes down, for SYML-Er2 and AZOL-Er3 the χT product slowly decreases and shows a sharper decrease below 50 K. The variation of the χT product with temperature is smoother for the Yb(III) complexes in all the temperature range. The changes in χT product with temperature are as expected due to the Boltzman depopulation of M_J sublevels and weak magnetic coupling. In particular for SYML-Yb2 and AZOL-Yb3, the smooth decrease in χT product is in agreement with the splitting of the M_J levels observed in the emission properties of the complexes. The susceptibility data for SYML-Yb2 and SYML-Er2 were fitted using the software PHI.[56] The program was designed for the treatment of systems containing orbitally degenerate and strongly anisotropic ions, through the inclusion of Spin-Orbit (SO) coupling and Crystal-Field (CF) effects using Steven's Operators and the following crystal field Hamiltonian:

$$\widehat{H}_{CF} = \sum_{i=1}^{N} \sum_{k=2,4,6} \sum_{q=-k}^{k} \sigma_i{}^k B_{k\,i}^q \theta_k \hat{O}_{k\,i}^q$$

In this Hamiltonian σi are the orbital reduction parameters *Bkqi* are the crystal field parameters, θk are the operator equivalent factors and $Okqi$ are operator equivalents. To describe the crystal field of lanthanide ions second, fourth and sixth rank operators are required. The ideal symmetry of the Ln(III) ions in SYML-Ln2 is low and the crystal field parameters were taken to be the same for the two lanthanide ions in SYML-Ln2 (Ln = Yb, Er), even though the two lanthanides are not equivalent. One lanthanide is octacoordinated in an ideal C2v N4O4 coordination sphere and the other is in a low symmetry Cs O5N2 coordination sphere. This a crude approximation necessary in order to avoid the overparametrization of the procedure and is usually accepted when using PHI to fit magnetic data for lanthanide complexes, with results similar to those reported by us here.[44,53,57,58] The $B_2^0, B_4^0\ B_6^0$ and B_6^4 crystal field parameters were used. The Ln-O-Ln angles (where O is the phenoxo bridging oxygen) are 110° and 108° in the crystallographically characterized SYML-Ln2 complexes. These values should result in very weak coupling (ferro or antiferromagnetic) between the lanthanide ions. Susceptibility and magnetization were fitted at the same time and the best set of parameters modelled both data sets. The exchange was surveyed with values between 1 cm^{-1} and -1 cm^{-1}. For SYML-YB2 the effects on magnetization and susceptibility were very subtle so J = 0 was chosen for the reported fitting. For SYML-Yb2 with g = 8/7 the crystal field parameters were $B_2^0\theta_2 = -0.77, B\ {}_4^0\theta_4 = 0.002$, $B_6^0\theta_6 = 0.021$ and $B_6^4\theta_6 = 0.059$ cm^{-1}. For SYML-Er2 the best fitting was obtained for g = 6/5, J = -0.24 cm^{-1} and the crystal field parameters $B_2^0\theta_2 = 15.88$, $B_4^0\theta_4 = 0.1846$, $B_6^0\theta_6 = 0.003$ and $B_6^4\theta_6 = -0.010$ cm^{-1}. The fittings are shown in Figure 6 as solid lines.

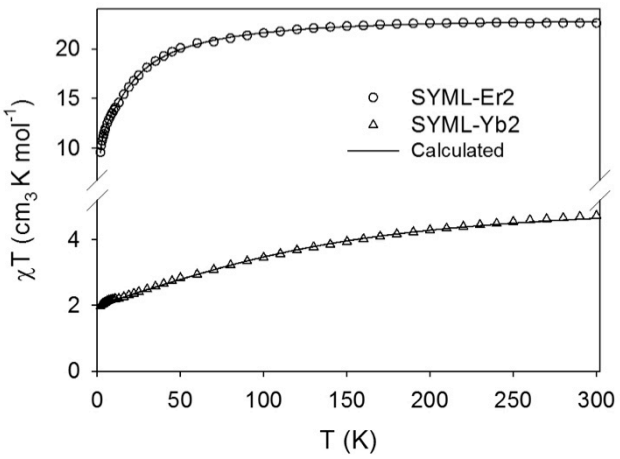

Figure 6. DC magnetic susceptibility plots shown as χT vs T plots for SYML-Er2 and SYML-Yb2 at applied fields of 5000 and 300 Oe. The solid lines are the bets fitting to the experimental data. See text for fitting parameters.

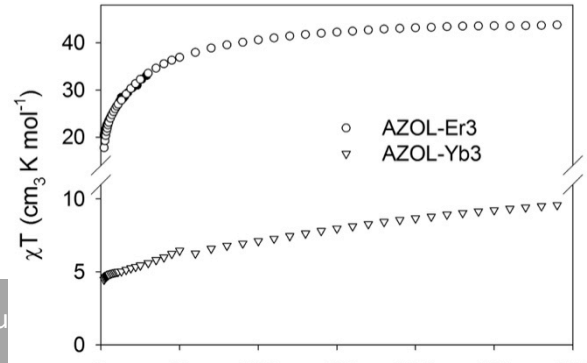

Figure 7. DC magnetic susceptibility plots shown as χT vs T plots for AZOL-Er3 and AZOL-Yb3 at applied fields of 3000 and 300 Oe.

Magnetization vs. field data at 2 K are shown in Supplementary information Figure S08, the fitting is shown as a solid line. In all cases the population of a magnetic state is observed. The magnetization values at 5 T and 2 K for SYML-Ln2 (Ln = Er, Yb) and AZOL-Ln3 (Ln = Er, Yb) are smaller than the expected values for two (SYML-Ln2) and four (AZOL-Ln3 with $Ln(NO_3)_3$) lanthanide ions due to crystal field splitting of the $^2F_{7/2}$ term for the Yb(III) complexes and the $^4I_{15/2}$ term for the Er(III) complexes. The crystal field parameters obtained from PHI can be used to obtain the energy splitting of the M_J sublevels. For SYML-Yb2 the lowest lying is $M_{J1} = M_{J2} = 1/2$, with $M_{J1} = 1/2$ and $M_{J2} = 5/2$ and $M_{J1} = M_{J2} = 1/2$ very close in energy (approx. 10 and 20 cm-1 above the ground state). The total splitting of the M_J sublevels is 793 cm^{-1}, in good agreement with the splitting observed in the NIR emission of the Yb(III) ions in SYML-Yb2 at room temperature. For SYML-Er2 the crystal field parameters obtained from PHI result in a $M_{J1} = 1/2$ and $M_{J2} = -1/2$ ground state level with a total splitting of approx. 590 cm^{-1}. Unfortunately, we have not been able to model the data for AZOL-Er3 and AZOL-Yb3, with four lanthanide ions each. The susceptibility and magnetization data suggest similar ground M_J state as those found for SYML-Ln2. For Ishikawa's $TBA[Yb(Pc)_2]$ and $TBA[Er(Pc)_2]$ the lowest M_J were reported as 5/2 and 1/2 respectively.[59]

Given the structural characteristics of these complexes the dynamic magnetic properties of SYML-Ln2 and AZOL-Ln3 were studied in the absence of DC applied fields. Previously reported salen double-decker type complexes by Li *et al* with Yb(III) were found to be field induced single molecule magnets with fast quantum tunnelling dominated relaxation of the magnetization.[33] In 2012 the first polynuclear field induced Yb(III) was reported by Murugesu and coworkers.[60] Most Yb(III) complexes reported as SMMs are mononuclear field-induced SMMs.[57,61,62]

AC magnetic susceptibility data were collected for the SYML-Ln2 and AZOL-Ln3 complexes for Ln = Er, Yb and are shown in Figures 8, 9 and 10. SYML-Yb2 shows no out-of-phase peak without an applied dc field, but upon application of a dc field the tail of an out-of-phase can be observed. The optimal field of 2000 Oe was chosen and ac data collected as a function of frequency for temperatures between 1.8 and 5 K, Figure 8. The out-of-phase ac susceptibility was fitted using the Debye model with $\alpha = 0.01$(5 K) to 0.34(1.8 K). The large values for α at low temperatures indicate a very broad distribution of relaxation times. The fitted out-of-phase ac susceptibility data are shown in Figure 9 as solid lines. The relaxation times extracted were fitted using the Arrhenius equation between 1.8 and 2.3 K to extract and effective barrier for the relaxation of the magnetization of 5.5 K for SYML-Yb2 (see supplementary material for the full fitting parameters).

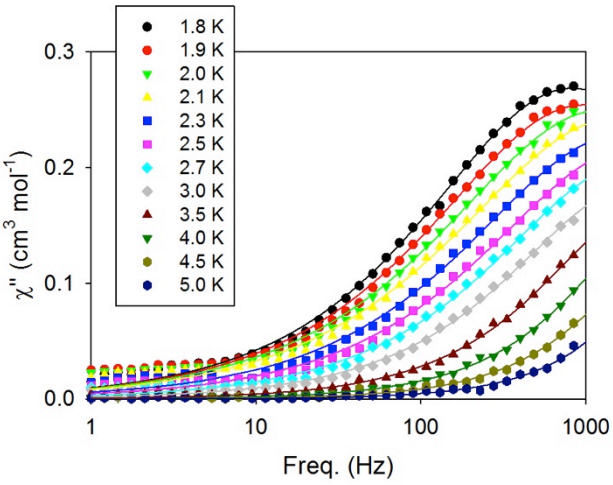

Figure 8. Out-of-phase AC magnetic susceptibility vs. frequency plot for SYML-Yb2 (DC field = 2000 Oe) between 1.8 and 5 K. The solid lines are fittings to a Debye model.

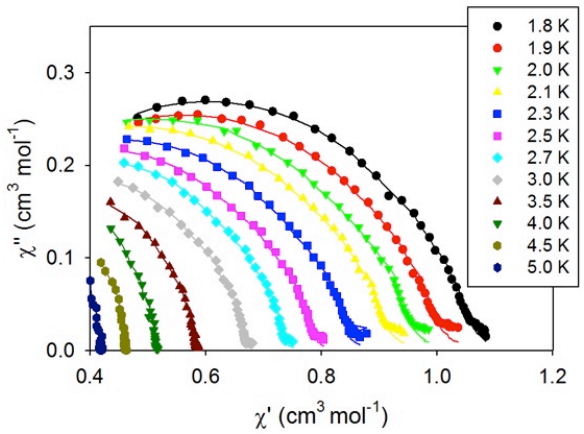

Figure 9. Argand plot for SYML-Yb2 at an applied dc field of 0.2 T. The solid lines are the best fitting to a Debye model. with parameters as shown in Table S01.

The tail of out-of-phase peaks is observed for SYML-Er2 in the absence of an applied dc field. At the optimal dc field of 2000 Oe there is a separation of out-of-phase peaks at temperatures below 3 K for slow relaxation processes and a tail assigned to a faster relaxation or QTM, as shown in Figure S11. The ac data for SYML-Er2 cannot be fitted to a simple Debye model or to a modified Debye model for two processes.[63] It is clear that the dynamics of relaxation for these species, with two lanthanide ions in different crystal fields are rather complicated.

For AZOL-Ln3 neither the Er(III) or Yb(III) analogues display out-of-phase ac signals down to 1.8 K without the application of a dc field. AZOL-Er3 in applied dc fields larger than 1000 Oe, displays the tail of an out-of-phase AC magnetic susceptibility peak when ac is plotted against temperature. Thus the new

complexes SYML-Ln2 (Ln = Er, Yb) and AZOL-Er3 complexes are new examples of lanthanide single-molecule magnets. The SYML ligand provides an appropriate crystal field for a field induced SMM in SYML-Yb2 and SYML-Er2 but AZOL fails to do so for AZOL-Yb3. The main difference between the ligands is the presence of a substituted diphenylazo group in AZOL or a naphtol in SYML, thus preparing the symmetric and asymmetric ligands we can effectively tune the crystal field.

Conclusions

Symmetric and asymmetric Schiff-base ligands with naphtyl groups, SYML and AZOL, have been prepared. The coordination complexes with Yb(III) and Er(III) have been prepared and characterized, SYML-Ln2 and AZOL-Er3 are new examples of SMMs. The crystal field was finely tuned from SYML to AZOL and this is reflected in the properties of the species. In summary, the complexes reported here are especially interesting due to three facts: i) the two lanthanide ions in SYML-Ln2 are not equivalent, this opens up possibilities of using the complex as two qubit quantum gate with two weakly coupled qubits; ii) the presence of the naphtyl and azo groups in the Schiff base ligands make these species interesting for surface deposition on metals and carbon based materials, and iii) multifunctionality has been achieved by combining the magnetic properties of 4f complexes with the dual emission properties: in the UV-vis of symmetric (SYML) and asymmetric (AZOL) Schiff base ligands and in the NIR of the lanthanides. A more detailed study of the emission properties of the complexes would be necessary in order to ascertain the efficiency of the sensitization process. Azo groups could be exploited for example to generate mechanical movement on a surface.[64]

Experimental

All chemicals were purchased from commercial sources and used as received. 1-(3-formyl-4-hydroxyphenylazo)-4-nitrobenzene was synthesized according to literature method.[35]

$C_{30}H_{21}N_5O_4$ (AZOL)

A mixture of 2-hydroxy-1-naphtaldehyde (1.72 g, 10 mmol) and *o*-phenylendiamine (1.08 g, 10 mmol) in anhydrous EtOH (80 mL) was heated to reflux for 6 h. After standing overnight, brown crystals formed. The product was filtered, washed with hexane, and dried in air. The yield was 53% (1.39 g). M.p. 171–172 °C. IR (KBr, cm^{-1}): 3473(s), 3373(s), 1613(s), 1556(s), 1491(s), 1469(w), 1317(s), 1182(s), 1156(s), 1134(w), 962(w), 817(s), 747(s). The precursor (0.524 g, 2 mmol) was placed in EtOH (20 mL). This slurry was heated to reflux until a solution was obtained. To this solution was added 1-(3-Formyl-4-hydroxyphenylazo)-4-nitrobenzene (0.542 g, 2 mmol) in small portions. When the addition was complete, the reaction mixture was stirred overnight. The mixture was filtered and the obtained solid was washed with hot ethanol (three times) and then with diethyl ether. The yield was 61%. m.p. 245–246 °C. AZOL was characterized by IR, ^{1}H-NMR and ESI-mass spectrometry. ^{1}H NMR (d_6-dmf): 7.0 (d); 7.2 (d); 7.35 (t); 7.45 (t); 7.55 (m); 7.65 (d); 7.85 (d); 7.95 (d); 8.15 (m); 8.5 (d); 8.6 (d); 8.7 (d); 9.4 (s); 9.9 (d). ^{13}C NMR (101 MHz, $CDCl_3$) δ (ppm): 170.44, 165.35, 163.17, 155.83, 155.03, 148.33, 145.50, 140.97, 139.85, 137.01, 133.16, 129.68, 129.42, 128.57, 128.14, 127.83, 127.39, 127.24, 124.74, 123.69, 123.16, 122.39, 119.65, 119.07, 119.00, 118.85, 118.80, 109.26. IR (KBr, cm^{-1}): 1621(s), 1582(s), 1517(s), 1482(w), 1339(s), 1291(w), 1173(w), 1143(w), 1104(s), 852(s), 830(w), 743(s), 688(w). ESI-MS: MW = 515.52 g/mol. Ms/z ($M+1H^+$) = 516.16.

$C_{28}H_{20}N_2O_2$ (SYML)

SYML (N,N'-bis(1-naphthaldiamine)-*O*-phenylenediamine) was synthesized according to literature methods.[36] *o*-Phenylendiamine (0.54 g, 5 mmol) is dissolved in 20 mL of ethanol. To this solution, 1.72 g (10 mmol) of 2-hydroxy-1-naphthaldehyde in 20 ml ethanol was added. The resulting solution was refluxed for 2 h. The obtained orange precipitate was filtered off and then dried with anhydrous diethyl ether. Yield: 74%. M.p. 210. ^{1}H NMR ($CDCl_3$): 7.1 (d); 7.3 (t); 7.4 (m); 7.5 (t); 7.7 (d); 7.8 (d); 8.1 (d); 9.4 (d). IR (KBr, cm^{-1}): 1621 (s), 1565 (s), 1469 (s), 1417 (w), 13218 (s), 1243 (w), 1173 (s), 969 (w), 878 (w), 821 (s), 734 (s). ^{13}C NMR (101 MHz, $CDCl_3$), δ (ppm): 168.91, 156.19, 139.74, 136.58, 133.17, 129.35, 128.02, 127.48, 127.35, 123.57, 121.99, 119.15, 118.99, 109.37. ESI-MS: ($C_{28}H_{20}N_2O_2$) MW = 416.47 g/mol. Ms/z ($M+1H^+$) = 417.16.

$[Er_3(AZOL)_4(H_2O)_2(NO_3)(Er(NO_3)_3)]$ (AZOL-Er3)

A stirred solution of ligand (0.1 g, 0.193mmol), $Er(NO_3)_3{\cdot}xH_2O$ (0.057 g, 0.128 mmol) in CH_3CN (20 mL) was heated under reflux. After added of Et_3N (81 µl, 0.868 mmol) color changed from brown to dark red and a precipitate formed. The resulting solution was stirred and heated at reflux for 6 h. The precipitate was filtered, washed with hot acetonitrile, and dried with anhydrous diethyl ether. Yield: 71.42% (0.08 g). AZOL-Er3 was characterized by IR, MALDI-TOF-mass spectrometry and EA. IR (KBr, cm^{-1}): 1608(s), 1573(s), 1517(s), 1473(w), 1382(s), 13308s), 1286(w), 1178(w), 1147(w), 1108(s), 986(w), 856(s), 739(s), 686(w). MALDI-TOF-MS: $[(C_{30}H_{19}N_5O_4)_4Er_3(NO_3)(H_2O)_2Er(NO_3)_3]$ MW = 2982 g/mol; Ms/z ($M-2H_2O-NO_3^-$-$Er(NO_3)_3$) = 2555; M/z ($M-Er(NO_3)_3+H^+$) = 2654. Elemental Analysis calculated for $[(C_{30}H_{19}N_5O_4)_4Er_3(NO_3)(H_2O)_2(Er(NO_3)_3]{\cdot}2(Et_2O)$: C, 48.78; H, 3.20; N, 10.67. Experimental: C 48.99; H 3.02; N 10.15 %.

$[Yb_3(AZOL)_4(H_2O)_2(NO_3)(Yb(NO_3)_3)]$ (AZOL-Yb3)

A stirred solution of ligand (0.1 g, 0.193 mmol), $Yb(NO_3)_3{\cdot}5H_2O$ (0.058 g, 0.128 mmol) in CH_3CN (20 mL) was heated under reflux. After addition of Et_3N (81 µl, 0.868 mmol) color changed from brown to dark red and precipitate formed. The resulting solution was stirred and heated at reflux for 6 h. The precipitate was filtered, washed with hot acetonitrile, and dried with anhydrous diethyl ether. Yield: 95%. The complex was characterized by IR, MALDI-TOF-mass spectrometry. IR (KBr, cm^{-1}): 1608(s), 1578(s), 1517(s), 1469(w), 1378(s), 1343(s), 1286(w), 1182(w), 1139(w), 1100(s), 991(w), 860(s), 821(w), 743(s), 686(w). MALDI-TOF-MS: $[(C_{30}H_{19}N_5O_4)_4Yb_3(NO_3)(H_2O)_2Yb(NO_3)_3]$ MW = 3014.29 g/mol; Ms/z ($M-2H_2O-NO_3^-$-$Yb(NO_3)_3$) = 2572; M/z ($M-Yb(NO_3)_3+H^+$) =

2671. Elemental analyses calculated for $[(C_{30}H_{19}N_5O_4)_4Yb_3(NO_3)(H_2O)_2(Yb(NO_3)_3]\cdot 4(H_2O)\cdot Et_2O$: C, 47.08; H, 3.06; N, 10.63. Experimental: C 46.45; H 2.80; N 10.19 %.

$[(C_{28}H_{18}N_2O_2)_3Er_2H_2O]$ (SYML-Er2)

A stirred solution of SYML (0.1 g, 0.2 mmol), $Er(NO_3)_3.xH_2O$ (0.07 g, 0.15 mmol) and Et_3N (100 µL, 0.6 mmol) in CH_3CN (20 mL) was heated under reflux for 6 h. After 5-6 days, orange crystals of SYML-Er2 were obtained by slow evaporation of solution. Yield: 93 %. IR (KBr, cm^{-1}): 1617(s), 1608(s), 1569(s), 1534(s), 1456(s), 1382(s), 1182(s), 982(w), 821(s), 726(s), 473(w). ESI-MS: $[(C_{28}H_{18}N_2O_2)_3Er_2H_2O]$ MW = 1592.9 g/mol. Ms/z ($M+1H^+-H_2O$) = 1578. Elemental Anal. Calc. for $[(C_{28}H_{18}N_2O_2)_3Er_2(H_2O)]\cdot 9H_2O\cdot 3MeCN$: C, 57.52; H, 4.45; N, 6.71. Experimental: C 57.28; H 4.16; N 6.51 %.

$[(C_{28}H_{18}N_2O_2)_3Yb_2H_2O]$ (SYML-Yb2)

A stirred solution of SYML (0.1 g, 0.2mmol), $Yb(NO_3)_3.5H_2O$ (0.058 g, 0.128mmol) and Et_3N (100 µl, 0.6mmol) in CH_3CN (20 mL) was heated under reflux for 6 h. After a day orange crystals of SYML-Yb2 were obtained by slow evaporation of solution. Yield: 76 %. IR (KBr, cm^{-1}): 1617(s), 1604(s), 1573(s), 1543(s), 1456(s), 1400(s), 1360(s), 1247(w), 1173(s), 1160(w), 982(s), 826(s), 730(s). ESI-MS: $[(C_{28}H_{18}N_2O_2)_3Yb_2(H_2O)]$ MW = 1607.49 g/mol. Ms/z ($M+1H^+-H_2O$) = 1590. Elemental Anal. Calc. for $[(C_{28}H_{18}N_2O_2)_3Yb_2(H_2O)]\cdot 4H_2O$:C, 59.98; H, 3.83; N, 5.00. Experimental: C 60.05 ; H 3.45; N 4.97 %.

$[NH_3py][(C_{28}H_{18}N_2O_2)_4Yb_3(NO_3)]$ (SYML-Yb3)

A stirred solution of SYML (0.1 g, 0.2 mmol), $Yb(NO_3)_3.5H_2O$ (0.058 g, 0.128mmol) and Et_3N (100 µl, 0.6mmol) in CH_3CN (20 mL) was heated under reflux for 6 h. 2-Aminopyridine (NH_2py) was added to the resulting cooled solution (excess, 0.06 g, 0.6 mmol). After 5-7 days, yellow crystals of SYML-Yb3 were obtained along with orange crystals of SYML-Yb2. The crystals were separated manually and characterized by single-crystal X-ray diffraction.

$[NH_3py][(C_{28}H_{18}N_2O_2)_4Er_3(NO_3)]$ (SYML-Er3)

A stirred solution of SYML (0.1 g, 0.2 mmol), $Er(NO_3)_3.xH_2O$ (0.07 g, 0.15 mmol) and Et_3N (100 µl, 0.6 mmol) in CH_3CN (20 mL) was heated under reflux for 6 h. 2-Aminopyridine (NH_2py) was added to the resulting cooled solution (excess, 0.06 g, 0.6 mmol). After 5-7 days, yellow crystals of SYML-Er3 were obtained along with orange crystals of SYML-Er2 after addition of 2 mL of THF. The crystals were separated manually and characterized by single-crystal X-ray diffraction.

Single crystal diffraction data for all the compounds were collected on a Bruker APEXII SMART diffractometer at the Facultat de Química, Universitat de Barcelona, using a 30 microfocus Molybdenum kα radiation source. The structures were solved by direct methods or intrinsic phasing (SHELXS97, SHELXT-2014) and refined on F2 (SHELX-97). Cif files can be obtained free of charge from the Cambridge Crystallographic Data Centre (CCDC https://summary.ccdc.cam.ac.uk/structure-summary-form, deposit codes: 1500647-1500650). Hydrogen atoms were included on calculated positions, riding on their carrier atoms. Infra-Red spectra were performed on a Thermo scientific AVATAR 330 FT-IR; Fluorescence measures were taken in a NanoLogTM-Horiba JobinYvon iHR320 spectrophotometer and fluorescein was used as standard to calculate quantum yields; UV-Vis spectra were acquired in a Cary 100 Scan from Varian. Irradiation of the samples was done with an ASAHI MAX 303 Xenon lamp. Elemental analyses were carried out at the CCiT-UB and CSIC. Mass spectrometry data were collected at the Unitat d'Espectrometria de Masses (CCiTUB). Magnetic measurements on crushed polycrystalline, vacuum dried samples (SQUID magnetometer equipped with a 5T magnet, diamagnetic correction applied using Pascal's constants) were done at the Servei de Mesures Magnètiques of CCiT-UB. ^{1}H-NMR (Varian Unity 300 MHz on manual mode) were performed at the NMR service of CCiT-UB.

Acknowledgements

ECS acknowledges financial support from the Spanish Government Ministerio de Economía y Competitividad via FEDER Funding (CTQ 2012-32247, CTQ2015-68370-P) and the Catalan Government agency AGAUR (project SGR-2014-129). SG and HK acknowledge support from Iranian Ministry of Science Research and Technology (MSRT) for funding for a stay at GMMF-UB.

Notes and references

1. R. Sessoli, H.-L. Tsai, A. R. Schake, S. Wang, J. B. Vincent, K. Folting, D. Gatteschi, G. Christou, and D. N. Hendrickson, *J. Am. Chem. Soc.*, 1993, **115**, 1804–1816.
2. W. Wernsdorfer, N. Aliaga-Alcalde, D. N. Hendrickson, and G. Christou, *Nature*, 2002, **416**, 406–9.
3. M. N. Leuenberger and D. Loss, *Nature*, 2001, **410**, 789–793.
4. F. Meier, J. Levy, and D. Loss, *Phys. Rev. Lett.*, 2003, **90**, 47901.
5. J. Lehmann, A. Gaita-Ariño, E. Coronado, and D. Loss, *J. Mater. Chem.*, 2009, **19**, 1672–1677.
6. P. Tyagi, *J. Mater. Chem.*, 2011, **21**, 4733.
7. A. Candini, S. Klyatskaya, M. Ruben, W. Wernsdorfer, and M. Affronte, *Nano Lett.*, 2011, **11**, 2634–2639.
8. L. Bogani and W. Wernsdorfer, *Nat. Mater.*, 2008, **7**, 179–186.
9. D. Gatteschi and R. Sessoli, *Angew. Chemie, Int. Ed.*, 2003, 268–297.
10. E. C. Sañudo and L. Rosado Piquer, *Dalt. Trans.*, 2015, **44**, 8771–8780.
11. D. N. Woodruff, R. E. P. Winpenny, and R. A. Layfield, *Chem. Rev.*, 2013, **113**, 5110–5148.
12. N. Ishikawa, M. Sugita, T. Ishikawa, S.-Y. Koshihara, and Y. Kaizu, *J. Am. Chem. Soc.*, 2003, **125**, 8694–8695.
13. C. Papatriantafyllopoulou, W. Wernsdorfer, K. A. Abboud, and G. Christou, *Inorg. Chem.*, 2011, **50**, 421–423.
14. F. Branzoli, P. Carretta, M. Filibian, G. Zoppellaro, M. J. Graf, J. R. Galan-Mascaros, O. Fuhr, S. Brink, and M. Ruben, *J. Am. Chem. Soc.*, 2009, **131**, 4387–4396.
15. M. Chen, E. C. Sañudo, E. Jiménez, S.-M. Fang, C.-S. Liu, and M. Du, *Inorg. Chem.*, 2014, **53**, 6708–6714.

16. D. Gatteschi, A. Cornia, M. Mannini, and R. Sessoli, *Inorg. Chem.*, 2009, **48**, 3408–3419.
17. J. Dreiser, C. Wäckerlin, M. E. Ali, C. Piamonteze, F. Donati, A. Singha, K. S. Pedersen, S. Rusponi, J. Bendix, P. M. Oppeneer, T. A. Jung, and H. Brune, *ACS Nano*, 2014, **8**, 4662–4671.
18. M. Mannini, F. Pineider, P. Sainctavit, C. Danieli, E. Otero, C. Sciancalepore, A. M. Talarico, M.-A. Arrio, A. Cornia, D. Gatteschi, and R. Sessoli, *Nat. Mater.*, 2009, **8**, 194–197.
19. V. Corradini, a Ghirri, E. Garlatti, R. Biagi, V. De Renzi, U. del Pennino, V. Bellini, S. Carretta, P. Santini, G. Timco, R. E. P. Winpenny, and M. Affronte, *Adv. Funct. Mater.*, 2012, **22**, 3706–3713.
20. R. Díaz-Torres, M. Menelaou, O. Roubeau, A. Sorrenti, G. Brandariz-de-Pedro, E. C. Sañudo, S. J. Teat, J. Fraxedas, E. Ruiz, and N. Aliaga-Alcalde, *Chem. Sci.*, 2016, **7**, 2793–2803.
21. A. Urtizberea and O. Roubeau, *Chem. Sci.*, 2017, **0**, 1–6.
22. Y. Bi, C. Chen, Y. Zhao, Y. Zhang, S.-D. Jiang, B.-W. Wang, J. Han, J. L. Sun, Z. Bian, Z. Wang, and S. Gao, *Chem. Sci.*, 2016, 5020–5031.
23. E. Merino, *Chem. Soc. Rev.*, 2011, **40**, 3835–3853.
24. F. Yang, P. Yan, Q. Li, P. Chen, and G. Li, *Eur. J. Inorg. Chem.*, 2012, 4287–4293.
25. Q. Li, P. Yan, P. Chen, G. Hou, and G. Li, *J. Inorg. Organomet. Polym. Mater.*, 2012, **22**, 1174–1181.
26. C. Chen, H. Chen, P. Yan, G. Hou, and G. Li, *Inorganica Chim. Acta*, 2013, **405**, 182–187.
27. P.-F. Yan, S. Chen, P. Chen, J.-W. Zhang, and G.-M. Li, *CrystEngComm*, 2011, **13**, 36–39.
28. N. Koike, H. Uekusa, Y. Ohashi, C. Harnoode, and F. Kitamura, 1996, **1669**, 5798–5804.
29. F. Gao, X.-M. Zhang, L. Cui, K. Deng, Q.-D. Zeng, and J.-L. Zuo, *Sci. Rep.*, 2014, **4**, 5928.
30. Y. L. Chien, M. W. Chang, Y. C. Tsai, G. H. Lee, W. S. Sheu, and E. C. Yang, *Polyhedron*, 2015, **102**, 8–15.
31. H. Wang, W. Cao, T. Liu, C. Duan, and J. Jiang, *Chem. - A Eur. J.*, 2013, **19**, 2266–2270.
32. A. M. Abu-dief, R. Díaz-torres, E. C. Sañudo, L. H. Abdel-rahman, and N. Aliaga-alcalde, *Polyhedron*, 2013, **64**, 203–208.
33. T. Q. Liu, P. F. Yan, F. Luan, Y. X. Li, J. W. Sun, C. Chen, F. Yang, H. Chen, X. Y. Zou, and G. M. Li, *Inorg. Chem.*, 2015, **54**, 221–228.
34. J. D. Rinehart and J. R. Long, *Chem. Sci.*, 2011, **2**, 2078–2085.
35. H. Khanmohammadi and F. Khodam, *J. Mol. Liq.*, 2013, **177**, 198–203.
36. Z. Popović, V. Roje, G. Pavlović, D. Matković-Čalogović, and G. Giester, *J. Mol. Struct.*, 2001, **597**, 39–47.
37. H. M. D. Bandara and S. C. Burdette, *Chem. Soc. Rev.*, 2012, **41**, 1809–25.
38. N. Aliaga-Alcalde, L. Rodríguez, M. Ferbinteanu, P. Höfer, and T. Weyhermüller, *Inorg. Chem.*, 2012, **51**, 864–873.
39. R. Van Deun, P. Fias, P. Nockemann, K. Van Hecke, and L. Van Meervelt, 2006, **45**, 1–5.
40. A. J. Amoroso and S. J. a Pope, *Chem. Soc. Rev.*, 2015, **44**, 4723–42.
41. C. Görller-Walrand and K. Binnemans, *Handbook on the Physics and Chemistry of Rare Earths, Vol. 25*, 1998.
42. H. Cui, T. Otsuka, A. Kobayashi, N. Takeda, M. Ishikawa, Y. Misaki, and H. Kobayashi, *Inorg. Chem.*, 2003, **42**, 6114–22.
43. F. R. Gonçalves e Silva, O. L. Malta, C. Reinhard, H. U. Güdel, C. Piguet, J. E. Moser, and J. C. G. Bünzli, *J. Phys. Chem. A*, 2002, **106**, 1670–1677.
44. F. Pointillart, B. Le Guennic, S. Golhen, O. Cador, O. Maury, and L. Ouahab, *Chem. Commun. (Camb).*, 2013, **49**, 615–7.
45. G. Xiong, X.-Y. Qin, P.-F. Shi, Y.-L. Hou, J.-Z. Cui, and B. Zhao, *Chem. Commun. (Camb).*, 2014, **50**, 4255–4257.
46. G. Cosquer, F. Pointillart, J. Jung, B. Le Guennic, S. Golhen, O. Cador, Y. Guyot, A. Brenier, O. Maury, and L. Ouahab, *Eur. J. Inorg. Chem.*, 2014, 69–82.
47. K. Soussi, J. Jung, F. Pointillart, B. Le Guennic, B. Lefeuvre, S. Golhen, O. Cador, Y. Guyot, O. Maury, and L. Ouahab, *Inorg. Chem. Front.*, 2015, **2**, 1105–1117.
48. F. Pointillart, B. Le Guennic, T. Cauchy, S. Golhen, O. Cador, O. Maury, and L. Ouahab, *Inorg. Chem.*, 2013, **52**, 5978–5990.
49. Q.-W. Li, J.-L. Liu, J.-H. Jia, Y.-C. Chen, J. Liu, L.-F. Wang, and M.-L. Tong, *Chem. Commun.*, 2015, **51**, 10291–10294.
50. Z.-H. Zhang, Y. Song, T. Okamura, Y. Hasegawa, W.-Y. Sun, and N. Ueyama, *Inorg. Chem.*, 2006, **45**, 2896–902.
51. X. P. Yang, R. A. Jones, M. M. Oye, A. L. Holmes, and W. K. Wong, *Cryst. Growth Des.*, 2006, **6**, 2122–2125.
52. P.-F. Yan, S. Chen, P. Chen, J.-W. Zhang, and G.-M. Li, *CrystEngComm*, 2011, **13**, 36.
53. J. Ruiz, G. Lorusso, M. Evangelisti, E. K. Brechin, S. J. A. Pope, and E. Colacio, *Inorg. Chem.*, 2014, **53**, 3586–3594.
54. K. S. Pedersen, J. Dreiser, H. Weihe, R. Sibille, H. V. Johannesen, M. A. S??rensen, B. E. Nielsen, M. Sigrist, H. Mutka, S. Rols, J. Bendix, and S. Piligkos, *Inorg. Chem.*, 2015, **54**, 7600–7606.
55. S. Dang, Q. Liu, K. Liu, Z. Guo, L. Sun, S. Song, and H. Zhang, *Cryst. Growth Des.*, 2010, **10**, 4662–4667.
56. N. F. Chilton, R. P. Anderson, L. D. Turner, A. Soncini, and K. S. Murray, *J. Comput. Chem.*, 2013, **34**, 1164–1175.
57. A. Lannes and D. Luneau, *Inorg. Chem.*, 2015, **54**, 6736–6743.
58. M. A. Aldamen, S. Cardona-Serra, J. M. Clemente-Juan, E. Coronado, A. Gaita-Ariño, C. Martí-Gastaldo, F. Luís, and O. Montero, *Inorg. Chem.*, 2009, **48**, 3467–3479.
59. N. Ishikawa, M. Sugita, T. Okubo, N. Tanaka, T. Iino, and Y. Kaizu, *Inorg. Chem.*, 2003, **42**, 2440–2446.
60. P.-H. Lin, W.-B. Sun, Y.-M. Tian, P.-F. Yan, L. Ungur, L. F. Chibotaru, and M. Murugesu, *Dalt. Trans.*, 2012, **41**, 12349–12352.
61. M. Menelaou, F. Ouharrou, L. Rodríguez, O. Roubeau, S. J. Teat, and N. Aliaga-Alcalde, *Chemistry*, 2012, **18**, 11545–11549.
62. J. J. Baldoví, S. Cardona-Serra, J. M. Clemente-Juan, E. Coronado, A. Gaita-Ariño, and A. Palii, *Inorg. Chem.*, 2012, **51**, 12565–74.
63. Y.-N. Guo, G.-F. Xu, Y. Guo, and J. Tang, *Dalt. Trans.*, 2011, **40**, 9953.
64. H. Koshima, N. Ojima, and H. Uchimoto, *J. Am. Chem. Soc.*,

2009, **131**, 6890–6891.